Research Article

Abeer S. Aloufi*

Green synthesis of strontium-doped tin dioxide ($SrSnO_2$) nanoparticles using the *Mahonia bealei* leaf extract and evaluation of their anticancer and antimicrobial activities

https://doi.org/10.1515/gps-2022-8116
received September 22, 2022; accepted March 28, 2023

Abstract: In this study, a simple green method was employed to produce strontium (Sr)-doped-tin-dioxide (SnO_2) nanoparticles ($SrSnO_2$ NPs) using the *Mahonia bealei* leaf extract. The synthesized NPs were characterized with XRD, FE-SEM, FTIR, and PL spectroscopy measurements. $SrSnO_2$ NPs were analysed for antimicrobial and anticancer activities. The XRD analysis revealed that the synthesized samples exhibited a tetragonal rutile crystal structure type of tin oxide. The EDX spectrum conforms to the chemical composition and elemental mapping of $SrSnO_2$ NP synthesis. At 632 cm^{-1}, the O–Sn–O band was observed and chemical bonding was confirmed using an FTIR spectrum. The PL spectrum identified surface defects and oxygen vacancies. The $SrSnO_2$ NPs were tested against both Gram-positive and Gram-negative human pathogens. The synthesized nanoparticles exhibited effective antibacterial properties. The anticancer effects of $SrSnO_2$ nanoparticles were also assessed against MCF-7 cells, and growth was decreased with increasing concentrations of the nanoparticles. Dual staining revealed high apoptosis in $SrSnO_2$ NP-treated MCF-7 cells, proving its apoptotic potential. To conclude, we synthesized and characterized potential $SrSnO_2$ nanoparticles using a green approach from the *Mahonia bealei* leaf extract. Further, green $SrSnO_2$ nanoparticles showed significant antibacterial and anticancer properties against breast cancer cells (MCF-7) through apoptosis, which suggests a healthcare application for these nanoparticles.

Keywords: green synthesis, antibacterial, tin oxide nanoparticles, *Mahonia bealei*, anticancer

Abbreviations

$SrSnO_2$ NPs	strontium (Sr)-doped tin dioxide nanoparticles
UV	ultraviolet
XRD	X-ray diffraction
SEM	scanning electron microscopy
TEM	transmission electron microscopy
MG/L	part per million

1 Introduction

Tin oxide nanoparticles (SnO_2 NPs) have recently received increasing interest due to their extraordinary chemical, physical, and biological properties, most notably their excellent antibacterial activity. It is an N-type semiconductor with a wide bandgap and the most promising material owing to its unique physicochemical properties. On the other hand, those methods require more energy and are more expensive. Additionally, both environmental and human health hazardous chemicals have been employed for tin oxide nanoparticle synthesis. As a result, there is a necessity to create safer eco-friendly tin oxide synthesis methods that avoid unsafe solvents and chemicals while maximizing the use of natural biodegradable materials [1].

Mahonia bealei is a significant member of the *Mahonia* genus and is widely employed in traditional Chinese medicine. Many bioactive compounds have been extracted from this plant and have beneficial properties. It is an ethnomedicinal plant [2] and therefore utilized in a variety of nations, including India, Malaysia, Mauritius, Bangladesh, Nepal, Mozambique, and Oman for abortion, asthma,

* **Corresponding author: Abeer S. Aloufi,** Department of Biology, College of Science, Princess Nourah bint Abdulrahman University, P.O. Box 84428, Riyadh 11671, Saudi Arabia,
e-mail: asaloufi@pnu.edu.sa

constipation, diarrhoea, earache, epilepsy, fever, ganglion, gum, and teeth disease, insect bites, headaches, decreased sugar levels, a mouth ulcer, acne, inflammatory bowel disease, syphilis, and healing of wounds, as well as an anti-helminthic, anti-parasite, aphrodisiac, dermatology ailment, emmenagogue, expectorant, and laxative [3–11]. The World Health Organization (WHO, 2022) has acknowledged that a reliable source of medicinal plants for traditional medicinal practices is based on plant sources for therapeutic applications [12].

The photocatalytic properties of tin oxide nanomaterials are highly promising candidates for microbial and cancer cell inactivation. Nanomaterials generate reactive oxygen species (ROS) and are strongly linked to antibacterial and anticancer activity [13]. This is because of their large surface areas, increased oxygen vacancies, reactant molecule diffusion, and active ion release. When tin oxide nanomaterials come into contact with light, they induce oxidative stress in cells, which leads to bacterial and cancer cell death. Tin oxide has, therefore, been employed to synthesize nanomaterials from both organic and inorganic substances due to these factors [14].

These ethnomedicinal plants can grow along the side of the road, in outdoor play areas, and in house compounds throughout settlements. In addition, they can be found in the wild or cultivated for personal use by some people. Moreover, the leaves contain valuable phytochemicals including alkaloids, anthraquinone, catechol, flavonoids, phenols, saponins, steroids, triterpenoids, and tannins [15]. The alkaline-earth metal was doped with tin oxide to enhance its physical, chemical, and biological properties. Technological applications can be expanded by doping with foreign metal ions. According to a literature report, charge compensation and ionic radius differences may arise through the doping of alkaline earth metals (Mg^{2+}, Ba^{2+}, Sr^{2+}), which can further boost the antibacterial activity [16].

In this study, the synthesis of alkaline-earth metal strontium-doped tin oxide NPs utilizing a simple green method has been carried out, which could increase optical efficiency. These nanoparticles open up additional opportunities for incorporating oxide nanoparticles into tin oxide. This will support a variety of fundamental and advanced concepts in a variety of applications. Though some research has been performed on the optical, antibacterial, and anticancer activity of $SrSnO_2$ NPs, there has been only limited research on the structural, optical, and antibacterial behaviours of $SrSnO_2$. As a result, we attempted to verify the impact of variations caused by the amalgamation of Sr ions into the tin oxide lattice site. Tin oxide NPs also play an important role in antibacterial and anticancer activities [17,18]. Previous studies reported that green synthesized cerium-doped tin oxide (Ce-SnO_2) nanoparticles exhibit talented anticancer effects against several tumours [19].

To synthesize and evaluate the properties of Sr ions on the structural, morphological, and elemental properties of $SrSnO_2$ nanoparticles, a Sr ion on tin oxide nanoparticles was hypothesized. Molecular characterization of $SrSnO_2$ NPs was performed using several characterization techniques. The antimicrobial properties of $SrSnO_2$ NPs were investigated. Additionally, their ability to inhibit the proliferation of cancer cells by inducing cytotoxicity has been investigated. The synthesized nanoparticles were further tested for their efficacy in inducing cytotoxicity via promoting apoptosis on MCF-7 cells.

2 Materials and methods

2.1 Materials

Chemicals such as tin chloride and strontium nitrate were acquired from Sigma Aldrich, USA. All the other required chemicals and reagents attained were of the analytical category.

2.2 Synthesis of green $SrSnO_2$ nanoparticles

Tin chloride and strontium nitrate were utilized as precursors without additional purification. Approximately, 10 g of fresh *M. bealei* leaves was boiled with deionized water (100 mL) for 10 min at 50–60°C. The suspension was filtered; in 100 mL of the *M. bealei* leaf extract, 0.2 M tin oxide was dissolved. For 6 h, this aqueous extract of tin chloride and *M. bealei* leaf was constantly shaken at 80°C. This resulted in a black precipitate, which was dried at 120°C. Similarly, 0.2 M tin chloride and 0.1 M strontium nitrate were dissolved in 100 mL of *M. bealei* leaf extract to synthesize $SrSnO_2$. On continuous stirring, a white precipitate was formed. This solution was constantly shaken for 6 h at 80°C. $SrSnO_2$ was obtained by drying the precipitate at 120°C. Finally, the nanopowder was annealed for 5 h at 800°C. As a result, tin oxide and $SrSnO_2$ NPs were produced [20].

2.3 Characterization of $SrSnO_2$ nanoparticles

An X'PERT PRO PANalytical XRD was employed to characterize the $SrSnO_2$ NPs. Diffraction patterns between 25°

and 80° were recorded with a monochromatic wavelength of 1.54. A NanoPlus DLS Nano Particle Sizer was utilized for the particle size comparison of $SrSnO_2$ NPs. FE-SEM (Carl Zeiss Ultra-55 FESEM) with EDAX and mapping analysis was employed to investigate the samples (model: Inca). A Perkin-Elmer spectrometer was utilized to obtain FT-IR spectra in the range of 400–4,000 cm^{-1}. The Cary Eclipse spectrometer was used to measure photoluminescence (PL) spectra [21].

2.4 Antibacterial activity of $SrSnO_2$ NPs

The well diffusion technique was used to determine the antibacterial properties of $SrSnO_2$ NPs against Gram-positive (*Staphylococcus aureus*, *Streptococcus pneumonia*, and *Bacillus subtilis*) and Gram-negative (*Klebsiella pneumonia*, *Escherichia coli*, and *Vibrio cholerae*) strains. To ensure homogeneous distribution of the inoculums, the bacteria were streaked onto the media plates (NA) twice, with each streak being rotated at 60°. After inoculation, sterile forceps were used to place wells containing 1, 1.5, and 2 $mg{\cdot}mL^{-1}$ $SrSnO_2$ NPs on the bacteria-inoculated plates. After that, the plates were incubated at 37°C for 24 h. Around the discs, the inhibition zone was noted and recorded. The positive control was amoxicillin (Hi-Media), which was tested against pathogens to compare the efficacy of the test samples.

2.5 Culturing of MCF-7 cells

The MCF-7 cells were cultured in Eagle's minimum essential medium supplemented with 1% antibiotics and 10% FBS. The culture medium with cells was incubated at 37°C by supplying 5% CO_2. A trypsin-EDTA solution containing 0.25% trypsin was used to perform experiments with sub-cultured cells at 80% confluency.

2.6 MTT assay

After seeding and incubating for 24 h at 37°C, the breast carcinoma MCF-7 cells were plated into a 96-well plate. $SrSnO_2$ NPs were applied in different dosages to the cells after the incubation period (5, 7.5, 10, 12.5, 15, and 20 $\mu M{\cdot}mL^{-1}$) for 24 h. The medium was later discarded; after adding serum-free culture medium to each well and MTT solution, the cells were incubated at 37°C in the dark for 3 h. The plates were incubated for 15 min after 150 µL of MTT was added to every well. The OD values in three replicates of each concentration were measured at 595 nm and used to determine the percentage of viable cells [22].

2.7 Dual staining assay

Dual staining using AO/EtBr stain was performed to evaluate the apoptotic potential of $SrSnO_2$ NPs in breast carcinoma cells, MCF-7. A 7.5 and 15 µM solution of $SrSnO_2$ NPs were used to treat the cells for 24 h. Then, the cells were rinsed with PBS and stained with a mixture of AO/EtBr (1:1). A fluorescence microscope was utilized to examine the stained cells [23].

2.8 Statistical analysis

GraphPad Prism version 6.02 software was employed to examine the values after the experiments were conducted. We analysed the data with a one-way ANOVA and subsequently the post hoc Duncan's test; significance we fixed at $P < 0.05$.

3 Results and discussion

3.1 Characterization of $SrSnO_2$ nanoparticles

The ultraviolet-visible absorbance spectrum of $SrSnO_2$ NPs is shown in Figure 1a. The absorption band edge values of the synthesized $SrSnO_2$ NPs were observed at 394 nm [24]. With the help of Planck's formula,

$$E_g = hc/\lambda = 1{,}243.1/\lambda \text{ (eV)} \quad (1)$$

where E_g is the band-gap energy (eV), h is Planck's constant (= 4.1357×10^{-15} eV s), and λ is the wavelength (nm). The band gap of nanomaterials was calculated in eV. Varshney et al. reported that the band gap of tin oxide/NiO_2 NPs was 3.132 eV compared to 3.3 eV for pure tin oxide NPs [25]. In the present work, a band gap of 3.1468 eV was observed for $SrSnO_2$ nanocomposites. The bandgap values of $SrSnO_2$ NPs are lower compared to that of tin oxide [26]. The effect

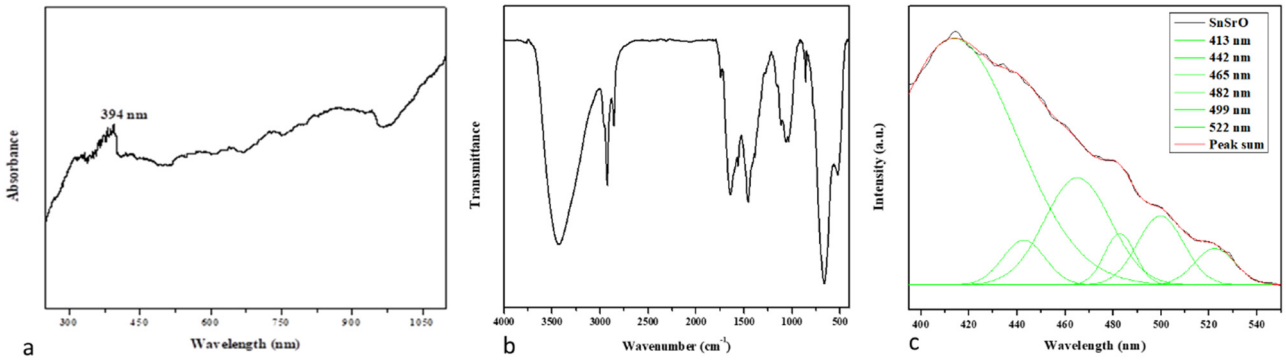

Figure 1: Spectral analysis of $SrSnO_2$ NPs: (a) UV-Vis spectrum, (b) FTIR spectrum, and (c) PL spectrum.

of different energy states in the valence band and conduction band of tin oxide is linked to a decrease in the band gap of NPs. As Sr^{2+} is added to the tin oxide lattice, oxygen vacancies are occupied to keep the local charge neutral, leading to these different energy states.

The wavenumbers 3,424, 2,923, and 2,853 cm^{-1} represent the stretching vibrations of O–H, and asymmetric and symmetric stretching of C–H, respectively. The aromatic functional groups are involved in the nanoparticle's reduction process observed at 1,639 and 1,561 cm^{-1} representing the primary amino acids I and II, respectively. The peaks ranging from 1,457 to 1,384 cm^{-1} represent the stretching vibrations of phenol (O–H) and C–H. The secondary amine found at 1,112 cm^{-1} acts as a capping agent. The C–O stretching changes were observed at 1,059 and 1,033 cm^{-1}. In the Sn–O mode, stretching was observed at 662 and 520 cm^{-1}. The FT-IR results display the presence of carboxyl (C–O), phenol (O–H), and proteins (amino acids) on the nanoparticle surface [27]. $SrSnO_2$ NPs were reduced and then stabilized by these phytocomponents (Figure 1b).

The PL spectrum of $SrSnO_2$ NPs with an excitation wavelength of 380 nm is shown in Figure 1c. The peaks in the PL emission spectrum of the $SrSnO_2$ sample were found at 413, 442, 465, 482, 499, and 522 nm. The violet emission, found at 413 nm, is accredited to the electron transition from the natural zinc interstitials' shallow donor level to the valence band's top level [28]. The blue emission peaks observed at 442, 465, 482, and 499 nm are allocated to single ionized Zn vacancies [29]. Finally, the green emission peak is located at 522 nm, and this emission corresponds to the single ionized oxygen vacancy [30].

Figure 2a represents the XRD pattern of the tin oxide and $SrSnO_2$ NPs that were synthesized using the green approach. Tin oxide NPs have XRD peaks that appear at

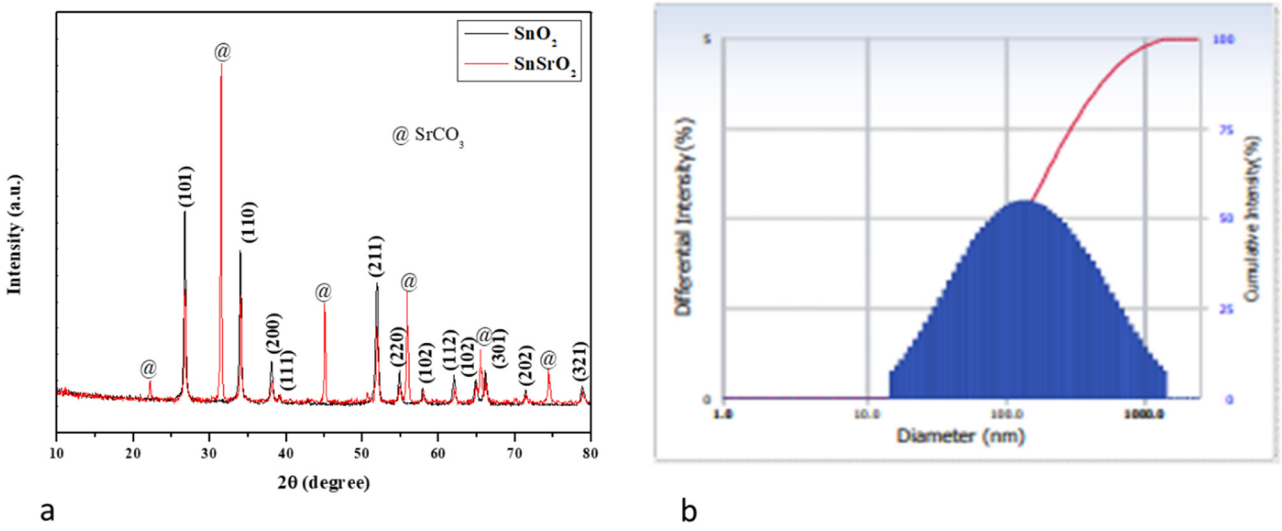

Figure 2: X-ray diffraction (a) and DLS (b) pattern of SnO_2 and $SrSnO_2$ NPs.

angles (2θ) of 26.53°, 33.94°, 37.95°, 38.94°, 51.99°, 54.87°, 57.99°, 62.01°, 64.64°, 66.15°, 71.42°, and 78.93°, and they correspond to the planes (110), (101), (201), (220), (220), (102), (301), respectively (JCPDS No. 41-1445). In addition, as per the JCPDS file No. 74-1491, the presence of some secondary phases associated with orthorhombic $SrCO_3$ [space group: *Pmcn* (62)] was discovered:

$$\text{Average crystallite size } (D) = \frac{0.9\lambda}{\beta\cos\theta} \quad (2)$$

where λ is the X-ray wavelength (= 1.54060), β is the angular peak width at half maximum (in rad), and θ is Bragg's diffraction angle. The average crystallite sizes of tin oxide and $SrSnO_2$ NPs were calculated to be 35.2 and 27.3 nm, respectively.

The hydrodynamic diameter of $SrSnO_2$ NPs was determined using dynamic light scattering to obtain the particle size (Figure 2b). The size of $SrSnO_2$ NPs was 143 nm; as the water medium surrounded the NPs, the DLS particle size was higher than XRD and TEM findings and is called hydrodynamic size.

The morphology, chemical composition, and elemental mapping of the synthesized $SrSnO_2$ NPs are shown in Figure 3a–c. As shown in the FESEM images, $SrSnO_2$ NPs exhibit a nanorod structure (Figure 3a). The average particle size was 200 nm. The chemical composition of $SrSnO_2$ NPs was demonstrated using the EDAX spectra and is shown in Figure 3b. In $SrSnO_2$ nanocomposites, the atomic percentages were as follows: 17.88% Sn, 9.88% Sr, and 72.24% O. The elemental mapping analysis revealed the presence of Sn, Sr, and O (Figure 3c). The NPs of $SrSnO_2$ exhibited uniform distribution of Sn, Sr, and O atoms throughout the structure.

3.2 Antimicrobial activity of $SrSnO_2$ NPs

The tin oxide and $SrSnO_2$ NPs were tested against *S. aureus*, *S. pneumonia*, *B. subtilis*, *K. pneumonia*, *E. coli*, and *V. cholerae* pathogens via the agar well diffusion method, as shown in Figure 4a. Figure 4a and b illustrates the zone of inhibition of tin oxide, $SrSnO_2$, and conventional antibiotics such as amoxicillin when treated with the bacterial strains. The $SrSnO_2$ NPs displayed higher antibacterial activity than tin oxide NPs. The bacterial inhibitory mechanism depends on the adsorption–desorption (A–D) and chemical–physical (C–P) activity between the $SrSnO_2$ NPs and various human pathogens. The interaction between the $SrSnO_2$ NPs and the human pathogens leads to distinct antibacterial activity. Each cytoplasmic lipid cell membrane produced A–D and C–P

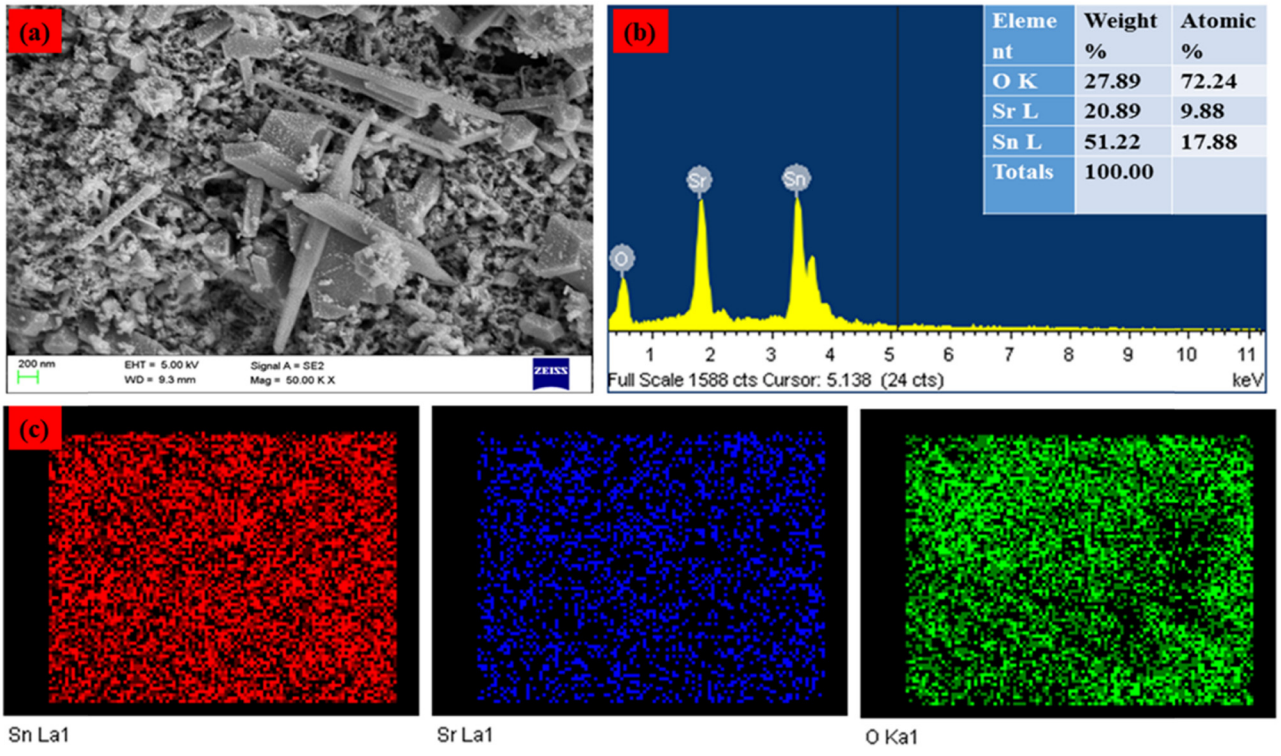

Figure 3: (a) FESEM image. (b) EDAX and (c) elemental mapping analysis of $SrSnO_2$ NPs.

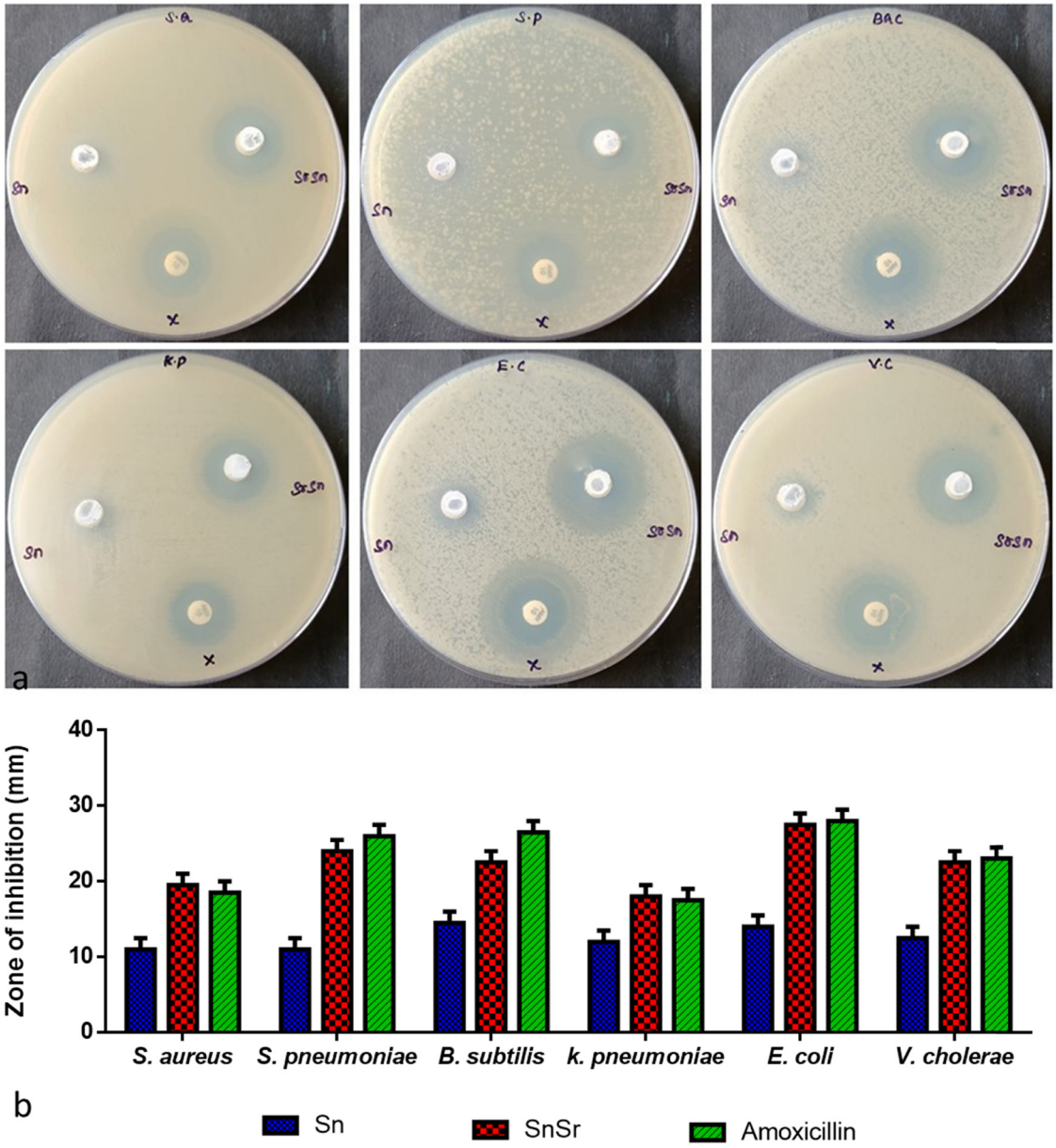

Figure 4: Antibacterial effect of $SrSnO_2$ NPs. Zone of inhibition (a) of Gram-positive bacteria (*S. aureus*, *S. pneumonia*, and *B. subtilis*) and Gram-negative bacteria (*K. pneumonia*, *E. coli*, and *V. cholerae*) was tested against $SrSnO_2$ NPs. Values represent mean ± SD of three experiments (b).

activities when $SrSnO_2$ NPs accumulated on the surface of each microbe. Nanomaterials synthesized through the green approach cause different disturbances on each cellular membrane, leading to cell death. The other antibacterial effects could be because varied amounts of active free radicals (ROSs) were formed on the cell walls during the contact, contributing to varying oxidative stress levels in the cells [31].

In previous studies, $SnCl_2H_2O$ was synthesized from leaf extracts of *Aloe barbadensis miller* as a precursor for SnO_2 nanoparticles. These nanoparticles were found to be spherical and ranged in size from 50 to 100 nm, and they revealed substantial antibacterial properties against *E. coli* and *S. aureus* [32]. Green synthesis of SnO_2 NPs can also be done efficiently and cheaply using the *P. amboinicus* leaf extract and $SnCl_2H_2O$ [33]. A previous study indicated that the *Nyctanthes arbortristis* (Parijataka) flower extract could reduce and stabilize SnO_2 nanoparticles and antimicrobial activity [34]. Previous studies demonstrated the antimicrobial activity of undoped and co-doped SnO_2 NPs against

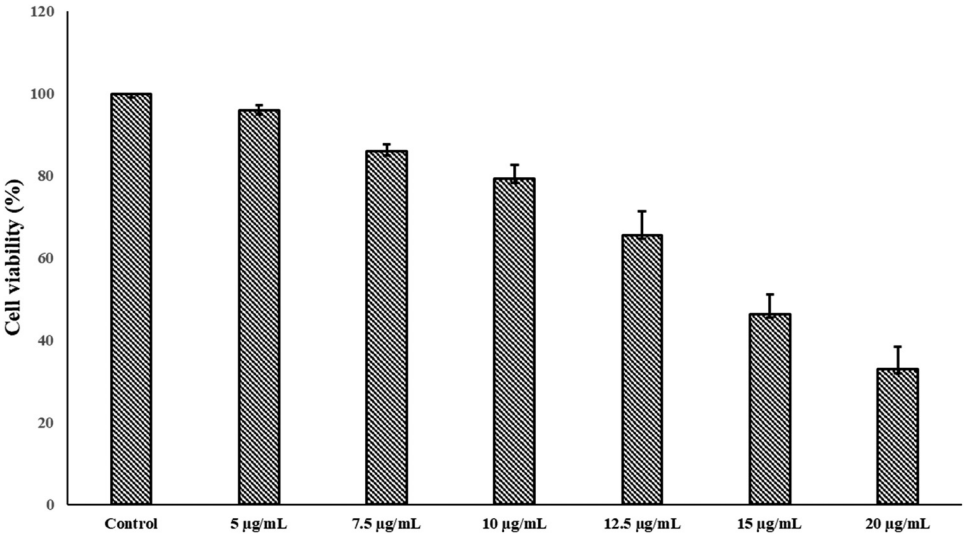

Figure 5: Cytotoxicity effects of $SrSnO_2$ NPs treated with MCF-7 cell line. The data were obtained for the treatment of 24 h and values represent mean ± SD of three experiments.

B. subtilis, *A. flavus*, *E. coli*, *A. niger*, and *C. albicans* [35]. In the past, similar studies reported that the formulation of SnO_2 NPs using the *P. pinnata* leaf extract revealed that the flower-like shape of NPs renders antibacterial properties against *K. pneumoniae*, *E. coli*, *S. aureus*, and *S. pyogenes*, which is comparable and even higher than tin oxide nanoparticles reported in previous studies [36]. Previously, similar studies reported that Ce-doped SnO_2 nanoparticles exhibited antimicrobial activity against *E. coli* and inhibited bacterial growth [37].

3.3 Cell viability assay

In this study, the *in vitro* cytotoxicity of $SrSnO_2$ NPs against MCF-7 cells was examined. The green-synthesized $SrSnO_2$ NPs were tested against MCF-7 cells. Cell growth decreased with increasing concentrations of $SrSnO_2$ NPs (5, 7.5, 10, 12.5, 15, and 20 $\mu g \cdot mL^{-1}$), which led to reduced cell viability. When $SrSnO_2$ NPs were treated with MCF cells for 48 h, the inhibitory concentration (IC_{50}) was 14 $\mu g \cdot mL^{-1}$ (Figure 5).

The particle size of $SrSnO_2$ NPs was 27.3 nm in this study. The XRD and PL results show several interstitial oxygen vacancies (O_i) at 522 nm for the sample's oxygen vacancies (O_v). The effects of the high number of ROS generated in $SrSnO_2$ NPs are responsible for the change. These defects allow more electron–hole pairs to migrate onto the nanomaterial matrix surface of $SrSnO_2$ NPs. While the electrons and holes can react with the superoxide anion ($\cdot O_2^-$), hydroxyl radicals (OH°), hydrogen peroxide (H_2O_2), and singlet oxygen ($^1O_2$) present in the aqueous environment of $SrSnO_2$ NPs may have contributed to ROS production. When free radicals contact the cellular environment, they can oxidize and reduce macromolecules such as nucleic acids, proteins, and lipids, leading to oxidative stress. Consequently, the cells are in a state of imbalance between ROS accumulation and the capacity of the biological system to rapidly eliminate reactive radicals or repair injury to tumour cells.

Tin oxide NPs were tested for cytotoxicity against liver cancer HepG2 cells using an aqueous extract of *A. squamosa*, and cells treated with tin oxide nanoparticles were inhibited in a dose- and time-dependent manner due to chromatin breakdown in the nucleus [38]. Tin oxide nanoparticles synthesized from the *Piper nigrum* seed extract demonstrated increased cytotoxicity against lung (A549) and colorectal (HCT116) cancer cell lines [39]. Tin oxide nanoparticles made from the *Pruni spinosae flos* aqueous extract exhibited substantial cytotoxicity against lung cancer A549 and CCD-39Lu cells in a concentration- and time-dependent manner, and the authors reported that the cytotoxicity was related to the accumulation ROS and increased oxidative stress [40]. In previous reports, *in vitro* cytotoxicity of green-synthesized undoped tin oxide and co-doped tin oxide NPs revealed a substantial mortality rate using the MTT assay, which further showed significant cytotoxicity and apoptosis in MCF-7 cells when compared with normal cell lines such as human lung fibroblast (WI38) and human amnion (WISH). The co-doped tin oxide NPs demonstrated more ROS accumulation than the undoped/doped tin oxide NPs [41].

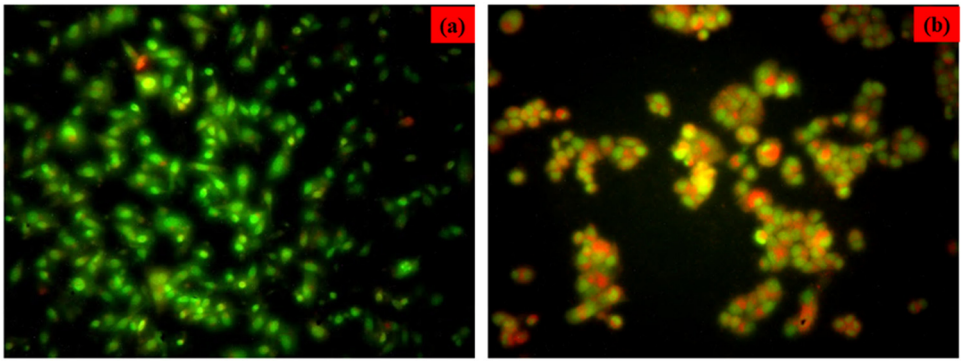

Figure 6: Apoptotic morphology of MCF-7 cells induced by $SrSnO_2$ NPs. (a) Control and (b) breast cancer (MCF-7) cells treated with IC_{50} concentration of $SrSnO_2$ NPs (14 μg·mL^{-1}) for 24 h and stained with dual dye AO/EB.

3.4 Acridine orange/ethidium bromide staining of $SrSnO_2$ NPs

Apoptotic changes and nuclear condensation are involved in $SrSnO_2$ NP cytotoxicity. Fluorescent DNA-binding AO/EB dyes were utilized to detect and quantify apoptosis induction and necrosis formation in MCF-7 cells before and after treatment with $SrSnO_2$ NPs. AO dye was absorbed by both living cells, as indicated by green fluorescence. On the other hand, EB dye only absorbs dead cells (red fluorescence). The bright green nuclei and orange cytoplasm were evenly distributed throughout viable cells. In the early stages of apoptosis, apoptosis-inducing cells appear to have a green-coloured nucleus because their membranes are still intact but their DNA breaks down, resulting in a green-coloured nucleus. A bright orange-coloured nucleus with dense chromatin reveals late apoptotic and necrotic cells (Figure 6a and b). The tin and oxygen vacancies in $SrSnO_2$ NPs are believed to be responsible for anticancer activity, leading to higher ROS production. Because of the composition of $SrSnO_2$ NPs, they can produce significant ROS spontaneously. Reeves et al. [42] reported a similar result, where a nanogel containing curcumin appeared more effective against MDA-MB 231 cells than curcumin alone. HT-29 cells treated with curcumin-containing chitosan NPs (CUR-CS-NPs) and free curcumin at 75 μM also displayed fragmentation of nuclei and irregular edges, clearly indicative of apoptosis [43]. MTT assays of $SrSnO_2$ nanoparticles were performed on MCF-7 cells and the nanoparticles showed potential anticancer activity. Nanoparticles also caused cancer cell death through apoptosis when stained with AO/EtBr. Overall, the nanoparticles demonstrated greater anticancer activity than tin oxide alone.

4 Conclusion

An eco-friendly green approach was employed to synthesize $SrSnO_2$ NPs, in which the *Mahonia bealei* leaf extract was used as a reducing and capping agent. The phase analysis results showed a tetragonal rutile-type structure and an average crystallite size of 27.3 nm. When compared to pure tin oxide crystals, $SrSnO_2$ NPs were reduced in size. UV absorption band edge values were observed at 394 nm. Moreover, the PL spectrum showed that a lot of oxygen vacancies induced ROS production and cell death. $SrSnO_2$ NPs displayed higher antibacterial activity than pure tin oxide nanoparticles. In addition, $SrSnO_2$ nanoparticles exhibited potent anticancer effects against breast cancer MCF-7 cells. In the near future, we believe that $SrSnO_2$ nanoparticles could serve as potential anticancer agents through further research.

Funding information: This research was supported by Princess Nourah bint Abdulrahman University Researchers Supporting Project number (PNURSP2023R357), Princess Nourah bint Abdulrahman University, Riyadh, Saudi Arabia.

Author contributions: Abeer S. Aloufi was solely responsible for the entire work.

Conflict of interest: The author states no conflict of interest.

References

[1] Soltys L, Olkhovyy O, Tatarchuk T, Naushad M. Green synthesis of metal and metal oxide nanoparticles: Principles of green chemistry and raw materials. Magnetochemistry. 2021;7(11):145.

[2] Kakar MU, Li J, Mehboob MZ, Sami R, Benajiba N, Ahmed A, et al. Purification, characterization, and determination of biological activities of water-soluble polysaccharides from *Mahonia bealei*. Sci Rep. 2022 May 17;12(1):8160. doi: 10.1038/s41598-022-11661-3. PMID: 35581215, PMCID: PMC9114413.
[3] Kumar D, Kumar A, Prakash O. Potential antifertility agents from plants: a comprehensive review. J Ethnopharmacol. 2012;140:1–32.
[4] Liu A, Liu S, Li Y, Tao M, Han H, Zhong Z, et al. Phosphoproteomics Reveals Regulation of Secondary Metabolites in *Mahonia bealei* Exposed to Ultraviolet-B Radiation. Front Plant Sci. 2022 Jan 11;12:794906. doi: 10.3389/fpls.2021.794906. PMID: 35087555, PMCID: PMC8787227.
[5] Vimala S. Kucing Galak. Malaysia: Institut Penyelidikan Perhutanan Malaysia; 2013.
[6] Savithramma N, Sulochana C, Rao K. Ethnobotanical survey of plants used to treat asthma in Andhra Pradesh, India. J Ethnopharmacol. 2007;113:54–61.
[7] Senthilkumar M, Gurumoorthi P, Janardhanan K. Some medicinal plants used by Irular, the tribal people of Marudhamalai hills, Coimbatore, Tamil Nadu. Nat Product Radiance. 2006;5:382–8.
[8] Huang Y, Jiang Z, Wang J, Yin G, Jiang K, Tu J, et al. Quality evaluation of *Mahonia bealei* (Fort.) carr. using supercritical fluid chromatography with chemical pattern recognition. Molecules. 2019 Oct 13;24(20):3684. doi: 10.3390/molecules24203684. PMID: 31614942; PMCID: PMC6832872.
[9] Hu W, Zhou J, Shen T, Wang X. Target-guided isolation of three main antioxidants from *Mahonia bealei* (Fort.) carr. leaves using hsccc. Molecules. 2019 May 17;24(10):1907. doi: 10.3390/molecules24101907. PMID: 31108973, PMCID: PMC6572348.
[10] Steyn DG. The presence of hydrocyanic acid in stock feeds and other plants. J S Afr Vet Assoc. 1938;9:60–4.
[11] Lingaraju D, Sudarshana M, Rajashekar N. Ethnopharmacological survey of traditional medicinal plants in tribal areas of Kodagu district, Karnataka, India. J Pharm Res. 2013;6:284–97.
[12] WHO Global Centre for Traditional Medicine. 2022. https://www.who.int/initiatives/who-global-centre-for-traditional-medicine.
[13] Fakhri A, Behrouz S, Pourmand M. Synthesis, photocatalytic and antimicrobial properties of SnO_2, SnS_2 and SnO_2/SnS_2 nanostructure. J Photochem Photobiol B. 2015 Aug;149:45–50. doi: 10.1016/j.jphotobiol.2015.05.017. Epub 2015 May 27, PMID: 26046748
[14] Li H, Li Q, Li Y, Sang X, Yuan H, Zheng B. Stannic oxide nanoparticle regulates proliferation, invasion, apoptosis, and oxidative stress of oral cancer cells. Front Bioeng Biotechnol. 2020;8:768. doi: 10.3389/fbioe.2020.00768.
[15] Hsieh CL, Yu CC, Huang YL, Chung KF. Mahonia vs. berberis unloaded: generic delimitation and infrafamilial classification of berberidaceae based on plastid phylogenomics. Front Plant Sci. 2022 Jan 6;12:720171. doi: 10.3389/fpls.2021.720171. PMID: 35069611; PMCID: PMC8770955.
[16] Ahmed A, Naseem Siddique M, Alam U, Ali T, Tripathi P. Improved photocatalytic activity of Sr doped SnO_2 nanoparticles: A role of oxygen vacancy. Appl Surf Sci. 2019;463:976–85.
[17] Venkatesan R, Rajeswari N. Poly (butylene adipate-co-terephthalate) bionanocomposites: effect of SnO_2 NPs on mechanical, thermal, morphological, and antimicrobial activity. Adv Compos Hybrid Mater. 2018;1(4):731–40.
[18] Ahamed M, Akhtar MJ, Khan MM, Alhadlaq HA. SnO_2-Doped ZnO/reduced graphene oxide nanocomposites: synthesis, characterization, and improved anticancer activity via oxidative stress pathway. Int J Nanomed. 2021;16:89.
[19] Prasanth M, Muruganandam G, Ravichandran K, Dayana Jeyaleela G, Shanthaseelan K, Priyadharshini BP. Anticancer activity of tin oxide and cerium-doped tin oxide nanoparticles synthesized from Ipomoea carnea flower extract. Biomed Biotechnol Res J. 2022;6:337–40.
[20] Buniyamin I, Akhir RM, Nurfazianawatie MZ, Omar H, Malek NSA, Rostan NF, et al. Aquilaria malaccensis and Pandanus amaryllifolius mediated synthesis of tin oxide nanoparticles: The effect of the thermal calcination temperature. Mater Today Proc. 2023;75:23–30.
[21] Elderdery AY, Alzahrani B, Alanazi F, Hamza SM, Elkhalifa AM, Alhamidi AH, et al. Amelioration of human acute lymphoblastic leukemia (ALL) cells by ZnO-TiO_2-Chitosan-Amygdalin nanocomposites. Arab J Chem. 2022;15(8):103999. doi: 10.1016/j.arabjc.2022.103999.
[22] Sudha D, Vairam S, Sarathbabu S, Senthil Kumar N, Sivasamy R, Jone Kirubavathy S, et al. 2-Methylimidazolium pyridine-2,5-dicarboxylato zinc (II) dihydrate: Synthesis, characterization, DNA interaction, anti-microbial, anti-oxidant and anti-breast cancer studies. J Coord Chem 74(16):2701–19. doi: 10.1080/00958972.2021.1981302.
[23] Zhang Q, Kandasamy K, Alyami NM, Alyami HM, Natarajan N, Elayappan PK. Influence of Padina gymnospora on Apoptotic Proteins of Oral Cancer Cells – a Proteome-Wide Analysis. Appl Biochem Biotechnol. 2022;194(12):5945–62. doi: 10.1007/s12010-022-04045-w.
[24] Mayandi J, Marikkannan M, Ragavendran V, Jayabal P. Hydrothermally synthesized Sb and Zn doped SnO_2 nanoparticles. J Nanosci Nanotechnol. 2014;2:707–10.
[25] Varshney B, Shoeb M, Siddiqui MJ, Azam A, Mobin M. Azadirachta indica (neem) leaves mediated synthesis of SnO_2/NiO nanocomposite and assessment of its photocatalytic activity. In AIP Conference Proceedings. Vol. 1953. Issue 1. AIP Publishing LLC; 2018, May. p. 030140.
[26] Matussin SN, Tan AL, Harunsani MH, Mohammad A, Cho MH, Khan MM. Effect of Ni-doping on properties of the SnO_2 synthesized using Tradescantia spathacea for photoantioxidant studies. Mater Chem Phys. 2020;252:123293.
[27] Bhavana S, Gubbiveeranna V, Kusuma CG, Ravikumar H, Sumachirayu CK, Nagabhushana H, et al. Facile green synthesis of SnO_2 NPs using vitex altissima (L.) leaves extracts: characterization and evaluation of antibacterial and anticancer properties. J Clust Sci. 2019;30(2):431–7.
[28] Teldja B, Noureddine B, Azzeddine B, Meriem T. Effect of indium doping on the UV photoluminescence emission, structural, electrical and optical properties of spin-coating deposited SnO_2 thin films. Optik. 2020;209:164586.
[29] Wang X, Wang X, Di Q, Zhao H, Liang B, Yang J. Mutual effects of fluorine dopant and oxygen vacancies on structural and

luminescence characteristics of F doped SnO_2 nanoparticles. Materials. 2017;10(12):1398.
[30] Ahmed A, Siddique MN, Alam U, Ali T, Tripathi P. Improved photocatalytic activity of Sr doped SnO_2 nanoparticles: a role of oxygen vacancy. Appl Surf Sci. 2019;463:976–85.
[31] Mostafa AM, Mwafy EA. Effect of dual-beam laser radiation for synthetic SnO_2/Au nanoalloy for antibacterial activity. J Mol Structure. 2020;1222:128913.
[32] Gowri S, Gandhi RR, Sundrarajan M. Green synthesis of tin oxide nanoparticles by *Aloe vera*: structural, optical and antibacterial properties. J Nanoelectron Optoelectron. 2013;8(3):240–9. doi: 10.1166/jno.2013.1466.
[33] Fu L, Zheng Y, Ren Q, Wang A, Deng B. Green biosynthesis of SnO_2 nanoparticles by plectranthus amboinicus leaf extract their photocatalytic activity toward rhodamine B degradation. J Ovonic Res. 2015;11(1):21–6.
[34] Rajiv Gandhi R, Gowri S, Suresh J, Selvam S, Sundrarajan M. Biosynthesis of tin oxide nanoparticles using corolla tube of nyctanthes arbor-tristis flower extract. J Biobased Mater Bioenergy. 2012;6(2):204–8.
[35] Khan SA, Kanwal S, Rizwan K, Shahid S. Enhanced antimicrobial, antioxidant, in vivo antitumor and in vitro anticancer effects against breast cancer cell line by green synthesized un-doped SnO_2 and Co-doped SnO_2 nanoparticles from Clerodendrum inerme. Microb Pathog. 2018;125:366–84. doi: 10.1016/j.micpath.2018.09.041.
[36] Fatimah I, Purwiandono G, Hidayat H, Sagadevan S, Mohd Ghazali SA, Oh WC, et al. Flower-like SnO_2 nanoparticle biofabrication using *Pometia pinnata* leaf extract and study on its photocatalytic and antibacterial activities. Nanomaterials (Basel). 2021 Nov 10;11(11):3012. doi: 10.3390/nano11113012. PMID: 34835776, PMCID: PMC8623890.
[37] Bhawna, Choudhary AK, Gupta A, Kumar S, Kumar P, Singh RK, et al. Synthesis, antimicrobial activity, and photocatalytic performance of Ce doped SnO_2 nanoparticles. Front Nanotechnol. 2020 Nov 19;2:595352.
[38] Roopan SM, Kumar SHS, Madhumitha G, Suthindhiran K. Biogenic-production of SnO_2 nanoparticles and its cytotoxic effect against hepatocellular carcinoma cell line (HepG2). Appl Biochem Biotechnol. 2015;175(3):1567–75. doi: 10.1007/s12010-014-1381-5.
[39] Tammina SK, Mandal BK, Ranjan S, Dasgupta N. Cytotoxicity study of Piper nigrum seed mediated synthesized SnO_2 nanoparticles towards colorectal (HCT116) and lung cancer (A549) cell lines. J Photochem Photobiol B. 2017;166:158–68. doi: 10.1016/j.jphotobiol.2016.11.017.
[40] Dobrucka R, Dlugaszewska J, Kaczmarek M. Cytotoxic and antimicrobial effect of biosynthesized SnO_2 nanoparticles using *Pruni spinosae* flos extract. Inorg Nano-Metal Chem. 2018;48(7):367–76. doi: 10.1080/24701556.2019.1569054.
[41] Khan SA, Kanwal S, Rizwan K, Shahid S. Enhanced antimicrobial, antioxidant, in vivo antitumor and in vitro anticancer effects against breast cancer cell line by green synthesized un-doped SnO_2 and Co-doped SnO_2 nanoparticles from *Clerodendrum inerme*. Microb Pathog. 2018;125:366–84. doi: 10.1016/j.micpath.2018.09.041.
[42] Reeves A, Vinogradov SV, Morrissey P, Chernin M, Ahmed MM. Curcumin-encapsulating nanogels as an effective anticancer formulation for intracellular uptake. Mol Cell Pharmacol. 2015;7(3):25.
[43] Chuah LH, Roberts CJ, Billa N, Abdullah S, Rosli R. Cellular uptake and anticancer effects of mucoadhesive curcumin containing chitosan nanoparticles. Colloids Surf B Biointerfaces. 2014;116:228–36.